Holography : noise in measurements from digital holographic interferometry

Pascal Picart
Erwan Meteyer
Felix Foucart
Charles Pezerat

22.07.2024

Table des matières

I.Présentation

Module :

Holography : noise in measurements from digital holographic interferometry

Auteur(s) :

- *Pascal Picart*[1] - Laboratoire d'Acoustique - Institut d'Acoustique - Graduate School (IA-GS)- Le Mans Université
- Erwan Meteyer - Laboratoire d'Acoustique - Institut d'Acoustique - Graduate School (IA-GS)- Le Mans Université
- Félix Foucart - Laboratoire d'Acoustique - Institut d'Acoustique - Graduate School (IA-GS)- Le Mans Université
- Charles Pezerat - Laboratoire d'Acoustique - Institut d'Acoustique - Graduate School (IA-GS)- Le Mans Université

Résumé :

This course presents analytical modeling of the speckle decorrelation noise indigital Fresnel holographic interferometry. The theoretical analysis is carried out by consideringt he complex coherence factor between two speckled images from two digitally reconstructedholograms at two different instants. The expression giving the modulus of the coherence factor is established and depends on the local surface deformation and parameters from the holographics et-up. The analysis is supported by realistic simulations and experiments. Both simulations and experimental results exhibit a very good agreement with the theoretical prediction.

Mots-clés :

Holography, noise, digital holographic, interferometry

Pré-requis :

-

Objectif(s) pédagogique(s) :

-

Plan du cours :

- Introduction
- Theorical blackground
- Theorical modelling
- Confrontation to stimulations
- Experiments
- Conclusion

Conception & production :

Le Mans Université

Licence :

1 - pascal.picart@univ-lemans.fr

2 - http://www.gnu.org/licenses/fdl.txt

II.Cours

Holography is a very powerful method for imaging and metrology [1 [A new Microscopic Principle],2 [New techniques in wavefront reconstruction], 3 [Digital holography and three-dimensional display : Principles and Applictions]4 [New techniques in digital holography]]. When becoming digital [5 [Direct recording of hologram by a a CDD target and numerical reconstruction]], holographic recordings are able to directly yield the complex-valued wave front of any encoded object volume or surface. Holographic phase imaging measures the optical path length related to the scene of interest [6 [Handbook of Holographic Interferometry : Optical and Digital Methods]]. The relevant data is a wrapped in modulo 2π phase that can be advantageously used for several purposes : automatic refocusing [7 [Refocusing criterion via sparisty measurements in digital holography], 8 [Comparative analysis of autofocus functions in digital in-line phase-shifting holography], 9 [Quality assement of refocus criteria for particle imaging in digital off-axis holography]],tracking refractive index changes [10 [Measurement of the integral refractive index and dynamic cell morphometry of living cells with digitalholographic microscopy]], microscopy [11 [Three-dimensional micrscopy with phase-shifting digital holography], 12 [High-resolution quantitative phase-contrast microscopy by digital holography]], tomography [13 [Holographic tomography : techniques and biomedical applications]], roughness measurements [14 [Surface-roughness neasurement based on the intensity correlation function of scattered light under speckle-pattern illumination],15 [Roughness determination by speckle-wavelength decorrelation]], surface shape profiling [16 [Miniaturized digital holography sensor for distal three-dimensional endoscopy],17, [Surface topography measuremnt by frequency sweeping digital holography]18 [Inline application of digital holography]], remote metrology [19 [Remote metrology by comparative digital holography]], or also surface deformation measurements [20 [Twin-sensitivity measurement by spatial multiplexing of digitally recorded holograms], 21 [Deformation measurement by phase-shifting digital holography]22 [Mechanical behavior of CAD/CAM occlusal ceramic reconstruction assessed by digital color holography]]. The comparison of the optical phases extracted from two digital holograms at two different instants refers to digital holographic interferometry [4 [New techniques in digital holography],6 [Handbook of Holographic Interferometry : Optical and Digital Methods]]. The method of holographic interferometry has the advantage of being non-intrusive by the use of laser illumination but also to provide full-field measurements. In addition, with the advent of very high-speed sensors, both high spatial and temporal resolutions can be obtained [23 [Visualization of travelling waves propagating in a plate equipped with 2D ABH using wide-field holographic vibrometry]] . From the practical point of view, the phase change is of interest and is calculated by the modulo 2π subtraction of two phases at two instants. This phase is also known as the Doppler phase and we refer to this term in this course. Thus, the process of holographic interferometry is perfectly adapted to the measurement of deformations of any object when submitted to mechanical load [24 [Measuring shape and deformation of small objects using digital holography]], or to periodic or transient excitation such as vibrations [25 [Digital double pulse-TV holography], 26, [Transient vibration measurements using multi-pulse digital holography]27 [Separate recording of rationally related vibration frequencies using digital stroboscopic holographic interferometry], 28 [Digital stroboscopic holography setup for deformation measurement at both quasi-static and acoustic frequencies], 29 [Multi-point vibrometer based on high-speed digital in-line holography], 30 [Lock-in vibration retrieval based on high-speed full-field coherent imaging]]. However, the speckle pattern produced from the object is modified and changes from its initial state. This induces decorrelation noise in the Doppler phase, requiring advanced filtering in order to get noise-freephase data [31 [Quantitative appraisal for noise reduction in digital holographic phase imaging]] or amplitude images [32 [Reduction of speckle in digital holography by discrete Fourier filtering], 33 [Quasi noise-free digital holography], 34 [Comparative study of multi-look processing for phase map de-noising in digital Fresnel holographic interferometry]]. The probability density of the phase noise induced by the speckle decorrelation is governed by the modulus of the complex correlation coefficient be $|\mu|$tween the two speckle fields [31 [Quantitative appraisal for noise

reduction in digital holographic phase imaging],35 [Laser speckle and related phenomena],36 [Speckle Phenomena in Optics : Theory and Applications]]. Note that there are other uncertainty sources inducing speckle noise decorrelation in the measured Doppler phase from digital Fresnel holography. For example, speckle decorrelation may be due to laser wavelength change between exposures [37 [Reduction of speckle noise in multiwavelength contouring]], to defocusing of the reconstructed image [38 [Refocus criterion based on maximization of the coherence factor in digital three-wavelenght holographic interferometry]] (the reconstruction distance is "not good"), to saturation of the recorded holograms [39 [Experimental and theroretical of the pixel saturation effect in digital holography]], or also due to quantization with low number of bits [40 [Quality assessment of combined quantiziation-shot-noise induced decorrelation noise in high-speed digital holographic metrology]].

From the theoretical point of view, description of speckle decorrelation has to consider the complex coherence factor, μ, [36 [Speckle Phenomena in Optics : Theory and Applications]] between two speckle fields when experimental parameters do change. The speckle decorrelation was discussed in several papers, for example in [41 [Spectral correlation of partially or fully developped patterns generated by rough surfaces], 42, [Calculation of complex correlation coefficents of two speckle fields of different wavelengths, and their application to two-wavelength-measurement techniques]43 [Speckle at various plane in an optical system], 44 [Speckle decorrelation in surface profilometry by wavelength scanning interferometry], 45 [Theoretical analysis of surface-shape-induced decorrelation noise in multi-wavelength digital holography]], for the case of wavelength changes. The decorrelation in speckle interferometers was discussed fromt he point of view of the fringe visibility in the correlation fringes [46 [General analysis of fringe contrast in electonic speckle pattern interferometry], 47 [Maximal fraction of acceptable measurements in phase-shifting speckle interferometry: a theoretical study], 48 [Decorrelation and fringe visibility : on the limiting behavior of various electronic speckle-pattern correlation interferometers]]. This course aims at investigating the phase noise by considering the theoretical model for the complex correlation coefficient in the case of digital Fresnel holographic interferometry. The case of objects submitted to deformations between the two digitally recorded holograms is examined.

The course is organized as follows: section 1 presents the basic fundamentals of digital Fresnel holography and section 2 discusses on the theoretical modeling for the complex coherence factor. In section 3, simulations are carried out in order to compare results obtained with simulations and the analytical model, and finally section 4 provides experiments and comparisons with the predicted theory. Section 5 draws the conclusions of the study.

1. Theorical blackground

1.1. Digital Fresnel holography

Digital Fresnel holography is based on the coherent mixing from a reference optical path and from diffraction at surface/volume of any object illuminated by a laser beam. The specificity of Fresnel holography is that recording uses lens-less configuration as depicted in Fig. 1(a) ;

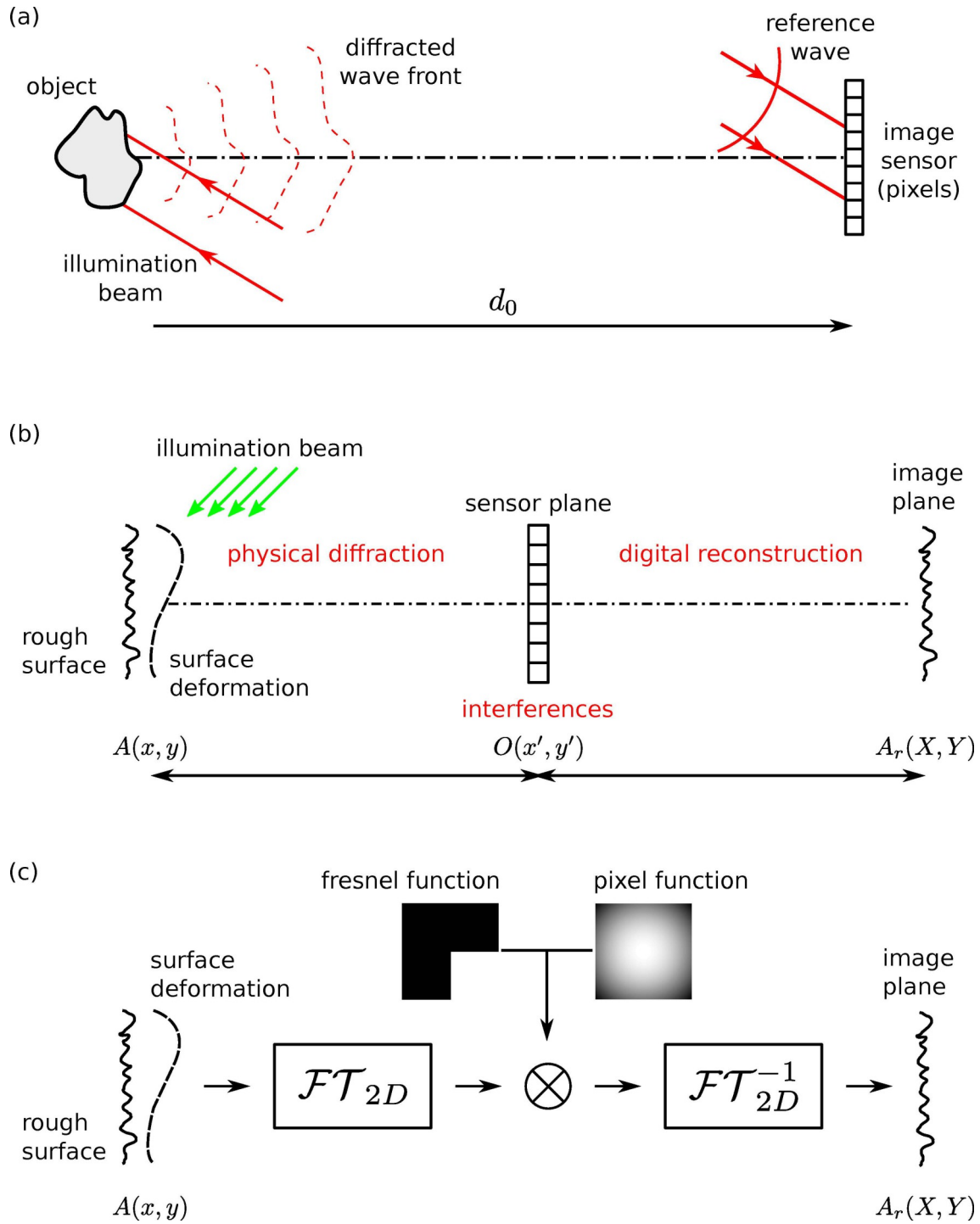

Fig. 1. (a) Basic scheme for digital Fresnel holography; the wave diffracted from the object propagates in the free space to the sensor area, and the reference wave impacts directly the matrix of pixels, (b) scheme of light propagation in digital holographic imaging with physical propagation from object to sensor plane, and numerical propagation from sensor plane to image plane, (c) numerical scheme for simulation of noisy Doppler phases by considering the point spread function of digital Fresnel holography (FT means Fourier Transform)

The mixing between the reference wave R and the object wave o results in the digital hologram expressed as :

The illuminated object surface is at distance d_0 from the recording sensor. The object wave diffracted to the sensor plane can be expressed with the Fresnel approximations by Eq. (2) [49 [Introduction To Fourier Optics]] $(i = \sqrt{-1})$:

The object wave front at the object plane is $A(x,y) = a(x,y)\exp[i\psi(x,y)]$, λ is the wavelength of light, a is related to the object reflectance and is ψ the optical phase related to the object surface shape and roughness. From the recorded holograms, the reconstruction of the object field at any distance d_r from the recording plane is given by he discrete Fresnel transform in Eq. (3) [5 [Direct recording of hologram by a a CDD target and numerical reconstruction],50 [General theoretical formulation of image formation in digital Fresnel holography]] :

with the FFT two-dimensional Fast Fourier Transform and the h_f Fresnel kernel defined by Eq.4,

With Eq.(3), the complex-valued optical field can be obtained. When considering two consecutive instants, the phase variation (Doppler phase) is obtained by subtracting the two phases extracted from the two digitally reconstructed optical fields at the two instants.

1.2. PSF of digital Fresnel Holography

When the reconstruction distance is set to $d_r = -d_0$ in Eq.(3), the initial object plane is recovered from the computation. In this case, the close relation between the initial object plane and the digitally reconstructed one can be described by the Point Spread Function (PSF) of digital Fresnel holography. Let $A(x,y)$ be the complex amplitude from the initial object plane and $A_r(X,Y)$ that of the complex-valued in-focus image calculated at the output of the reconstruction algorithm. Then, the two optical fields are linked by the convolution relation [49 [Introduction To Fourier Optics]], with $\mathrm{PSF}(x,y)$ being the Point Spread Function :

Basically, the full propagation scheme of digital Fresnel holography can be summarized in Fig. 1(b). The configuration is considered as lens-less, one half of the propagation physically exists (from the object to the sensor array), whereas the second half is pure numerical reconstruction from the sensor area to the image plane. By considering correct digital refocus, the general formulation of the can $\mathrm{PSF}(x,y)$ be written as ($\otimes$ means convolution product) [50 [General theoretical formulation of image formation in digital Fresnel holography],51 [Some opportunities for vibration analysis with time averaging in digital Fresnel holography]] :

where $\Pi_{\Delta_x,\Delta_y}(x,y)$ represents the active surface of pixels, expressed as :

and Δ_x, Δ_y are respectively the active width of the pixels in x and y directions. The second term $\tilde{W}_{NM}(x,y)$ corresponds to the filtering function induced by the discrete Fresnel transform. This term was demonstrated to be [50 [General theoretical formulation of image formation in digital Fresnel holography]]:

In Eq.(8), are N, M the number of pixels of the matrix sensor and p_x, p_y are the pixel pitches respectively in x and y directions, λ being the wavelength of light. Note that p_x, p_y and Δ_x, Δ_y are linked to the fill factor of the sensor by $\xi = \Delta_x\Delta_y / p_x p_y$. In this course, $\mathrm{sinc}(x) = \sin(x)/x$.

1.3. Decorrelation noise in phase measurements

As pointed out before, the Doppler phase suffers from noise due to the speckle decorrelation between the two instants, when the object surface is submitted to any change. The decorrelation noise has specific properties compared to other noise sources in imaging systems : first the noise does not follow Gaussian statistics, then it exhibits amplitude-dependent statistics, last, the noise is not stationary in the field of view. That makes the decorrelation speckle noise a very particular source of random fluctuations in coherent phase imaging. The probability density of this noise is given by [35 [Laser speckle and related phenomena]] :

with $\beta = |\mu|\cos(\epsilon)$. Eq.(9) depends on $|\mu|$ which is the modulus of the complex coherence factor of the two speckle fields at the two instants. The probability density is mapped for different values of $|\mu|$ in Fig. 2.

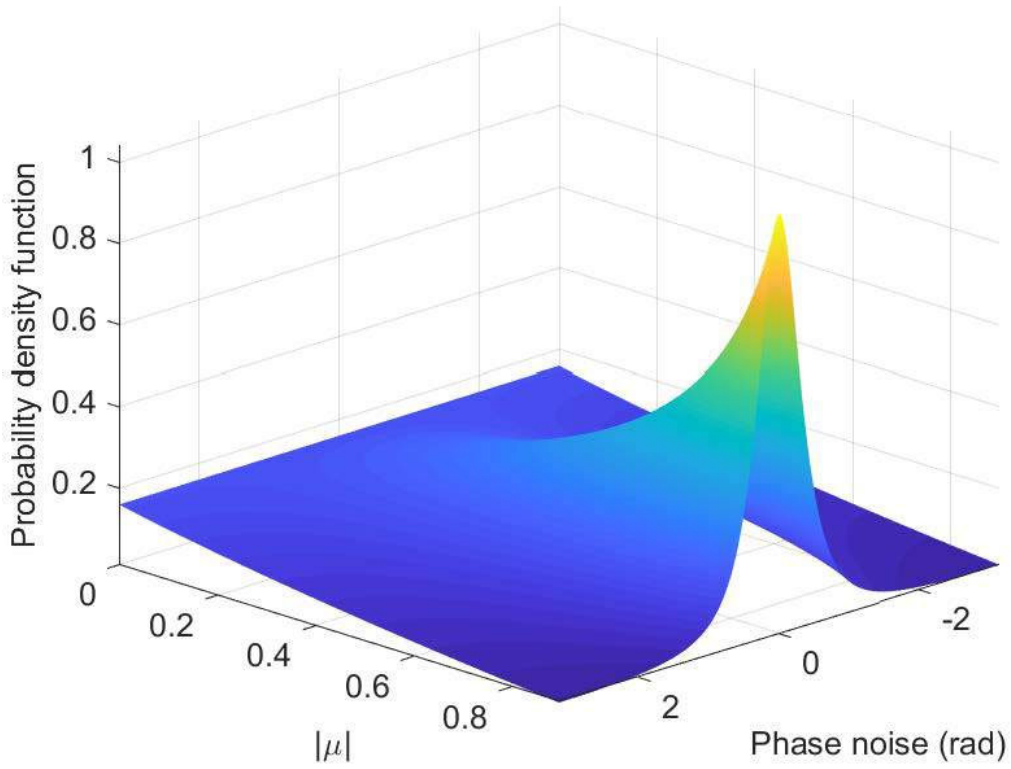

Fig. 2. Probability density function of the speckle decorrelation noise as depending on |□| .

As $|\mu|$ decreases, broadening of the probability density is observed. The higher the value of $|\mu|$ is, the less the signal is noisy and the more the curve tends to Gaussian shape. On the contrary, if $|\mu|$ decreases, the phase data will be more and more noisy and the noise will be uniformly distributed between π and π. The non-stationary property of the speckle phase noise can be appreciated with Fig. 3 which considers the case of the Doppler phase obtained between two different instants when a structure is vibrating. Figure 3(a) shows the modulo 2π noisy phase fringe pattern and Fig. 3(b) provides the denoised phase using the two-dimensional windowed Fourier transform [52 [Two-dimensional windowed Fourier transform for fringe pattern analysis: Principles, applications and implementations]]. The standard deviation and the value of $|\mu|$ both depend on the fringe density in Fig. 3(a). In order to get more quantitative noise appraisal, Fig. 3(c) provides the map of the noise in the phase map. The two patchs show local noise maps with different standard deviation and $|\mu|$.

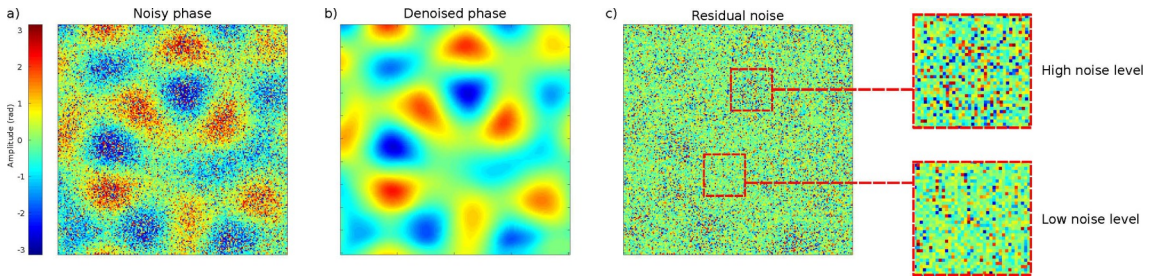

Fig. 3. Non-stationary property of the speckle phase noise, (a) mod 2□ noisy digital fringes, (b) noise map from (a), (c) standard deviation of noise for each patch, (d) modulus of the coherence factor for the same patches; the grids in (a),(b),(c),(d) indicate the patches in the phase data

One can observe that the speckle noise is not uniformly distributed over the field of view, but that it depends on the local fringe density, which is related to the elevation of the phase map. The elevation of the phase map is closely related to the displacement of the structure between the two exposures. The noise is stronger in the high displacement areas and less where there is no significant displacement. As can be observed, the areas in which the standard deviation is high in Fig. 3(c) is related to areas with high fringe density in Fig. 3(a), indicating a close link between the phase noise and the local slope of the surface deformation.

The standard deviation σ_ϵ of the decorrelation noise depends on the modulus of the complex coherence factor between the two speckle fields [36 [Speckle Phenomena in Optics : Theory and Applications]]. The relation is non trivial, but an approximate formula for σ_ϵ valid for $|\mu| \in [0.7; 1]$ was provided [38 [Refocus criterion based on maximization of the coherence factor in digital three-wavelenght holographic interferometry]] :

It follows that linking the fundamental parameters influencing $|\mu|$ is of major interest in order to be able to predict the noise standard deviation in the Doppler phase maps. Next section discusses on the theoretical expression of the modulus of the complex coherence factor by taking into account of the PSF of digital Fresnel holography.

2. Theorical modelling

2.1. Complex coherence factor of the digital images

The complex correlation coefficient is defined by the mutual intensity between the two image fields $A_r(\mathbf{X_1})$ and $A_r(\mathbf{X_1})$ obtained for two instants t_1 and $t_2 = t_1 + \Delta t$[36 [Speckle Phenomena in Optics : Theory and Applications],53 [Statistical optics]] :

where $\langle ... \rangle$ stands for statistical average. For the sake of compactness of the formulas, vector notation is adopted to designate the coordinates of a point located in the image plane (X, Y) , i.e. $\mathbf{X}$ and in the object plane $\mathbf{X}$, i.e.$\mathbf{X}$. The two terms in Eq. (11) obey the condition [36 [Speckle Phenomena in Optics : Theory and Applications]] :

meaning that the value of the complex correlation coefficient is normalized to 1 when no movement of the object is observed. In order to determine the expression on $\boldsymbol{\mu}$ the estimation of $\langle A_r(\mathbf{X_1}) A_r^*(\mathbf{X_2}) \rangle$ is required. One has:

In this way, the statistical average is applied only to the non-deterministic factor $\langle A(\mathbf{x_1})A^*(\mathbf{x_2})\rangle$. According to Ruffin et al.[41 [Spectral correlation of partially or fully developped patterns generated by rough surfaces],54 [Application of speckle-correlation methods to surface-roughness measurement: a theoretical study]], the phase of the object under illumination and observation can be written as :

with $k = 2\pi/\lambda$, θ_e and θ_o the illumination and observation angles of the surface [54 [Application of speckle-correlation methods to surface-roughness measurement: a theoretical study]]. In order to simplify Eq.(14), one notes $\Omega_z = k(\cos(\theta_e) + \cos(\theta_o)$ and $\Omega_x = k(\sin(\theta_e) + \sin(\theta_o))$, so that it reduces to :

The illumination of the object surface is considered as constant (illumination with a uniform extended light spot) to yield the amplitude of the object wave $a(\mathbf{x}) \simeq a$. The surface height at any instant is $h_z(\mathbf{x})$, while $\rho(\mathbf{x})$ corresponds to the roughness of the object surface.

Figure 4 depicts the notations for illumination, observation, surface height and roughness. The surface height may change between instant t_1 and t_2 because of the surface deformation in case where the object is submitted to loads (pneumatic, acoustic, mechanic, thermal, ...).

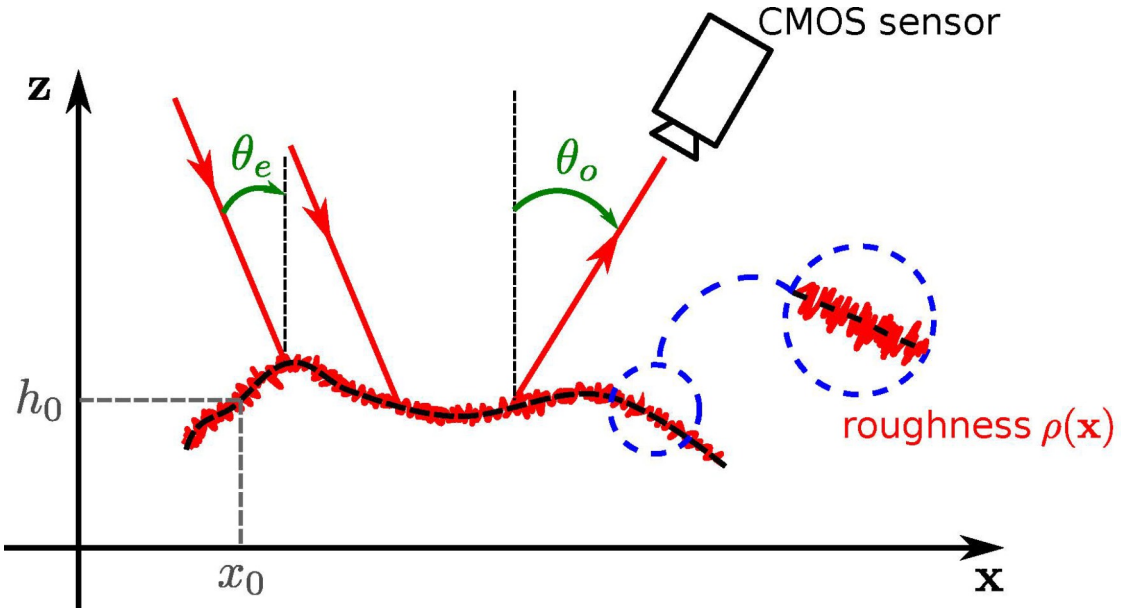

Fig. 4. Notations for illumination, observation, height and roughness of the object surface.

The roughness $\rho(\mathbf{x})$ is random and statistical approach has to be considered, whereas $h_z(\mathbf{x})$ is deterministic because it only depends on the surface height and deformation. It follows :

and therefore,

The joint-characteristic function of the roughness can be expressed as [43 [Speckle at various plane in an optical system],54 [Application of speckle-correlation methods to surface-roughness measurement: a theoretical study]] :

In Eq.(18),R_{hh} is the normalized surface roughness auto-correlation function. If the roughness standard deviation S_q is larger than the wavelength λ [55 [First-order probability density function of the laser speckle phase]] and the width of the roughness auto-correlation is narrower than the width of the PSF of the imaging system, Eq.(18) can be expressed as a Dirac distribution $\delta(\mathbf{x})$. One obtains after a limited expansion of the exponential function [41 [Spectral correlation of partially or fully developped patterns generated by rough surfaces],43 [Speckle at various plane in an optical system],54 [Application of speckle-correlation methods

to surface-roughness measurement: a theoretical study],56 [Space and wavelength dependence of speckle intensity]]

It comes :

It follows that the cross correlation of the two fields $A_r(\mathbf{X_1})$ and $A_r(\mathbf{X_2})$ does not depend on the surface roughness of the object, but only on the difference in elevation between the two instants.

2.2. Local surface deformation slopes

The deformation of the object can be seen as a local linear variation of the surface shape around its original position. In order to evaluate Eq.(20) and to obtain the expression of $\boldsymbol{\mu}$ as a function of the linear variation between the two consecutive instants, one considers the case ofthe out-of-plane surface deformation according to $h_z(x,y,t) = h_0 + \alpha_x(t)x + \alpha_y(t)y$. For thein-plane deformation, the coordinate is changing according to $x_0 + \beta_x(t)x$. So, $(\alpha_x(t), \alpha_y(t))$ are the local slopes due to out-of-plane deformation and $(\alpha_x(t), \alpha_y(t))$ is that due to in-plane deformation. It then comes (for fluidity of calculation $h_z(\mathbf{x},t) = h_0 + \alpha(t)\mathbf{x}$) :

giving,

Since the second integration is also a convolution product, one gets :

and then

The integral in Eq.(24) is the Fourier transform of the product of the two PSF evaluated at thespatial frequency $\mathbf{u} = \frac{\Omega_z}{2\pi}(\alpha(t_1) - \alpha(t_2)) + \frac{\Omega_x}{2\pi}(\beta_x(t_1) - \beta_x(t_2))$ depending on the deformation state at time t_1 and t_2. Noting $\Delta\alpha_{12} = \alpha(t_1) - \alpha(t_2)$ and $\Delta\beta_{12} = \beta_x(t_1) - \beta_x(t_2)$ respectively the local out-of-plane and in-plane slopes due to the surface deformation between instants t_1 andt_2, we have (⊗ stands for convolution product) :

where $p(\mathbf{u})$ is the Fourier transform of $\mathrm{PSF}(\mathbf{X})$.

2.3. Final expression of |μ|

For the sake of clarity, one notes $\mathbf{u}_{\alpha\beta} = \frac{\Omega_z}{2\pi}\Delta\alpha_{12} + \frac{\Omega_x}{2\pi}\Delta\beta_{12}$. Using Eq. (11) and Eq. (25) one obtains the expression of the complex correlation coefcient of the two felds which is expressed as a convolution product :

This expression is not easily manipulated as it is, except when performing numerical calculation of the convolution for special cases. However, an approximate expression for the modulus of the complex correlation coefficient can be provided by considering the sensor matrix as real-valued unction (which it is $a\ priori$). Thus, one gets :

The modulus $|\mu|$ depends on the slope variation between the two instants $\Delta\alpha_{12}$ and $\Delta\beta_{12}$. In addition,$|\mu|$ is directly proportional to the auto-correlation of the analog-digital pupil-type function of digital Fresnel holography. The PSF of the system being related to convolution of two functions (Eq.(6)), its Fourier transform is the multiplication of the Fourier transform of both functions. For the pixel function [51] [Some opportunities for vibration analysis with time averaging in digital Fresnel holography], one has (FT means Fourier Transform) :

Similarly with $\mathbf{U_x} = \dfrac{\mathbf{N}p_x}{\lambda d_0}$, one obtains for the filtering function of the Fresnel transform :

where $\mathbf{N}$ stands for N, M. The term in Eq. (27) is then :

Since the two shifted Dirac functions will compensate for after the convolution in Eq.(27), finally it comes for $|\mu|$:

Note that the key parameter $\mathbf{U_x} = \mathbf{N}\mathbf{p_x}/\lambda d_0$ included in Eq.(31) is the cut-off frequency of digital Fresnel holography and refers to the inverse as what is usually considered to be the spatial resolution of the digital holographic reconstruction $\rho_{\mathbf{x}} = 1/\mathbf{U_x} = \lambda d_0/\mathbf{N}\mathbf{p_x}$, [4 [New techniques in digital holography], 5 [Direct recording of hologram by a a CDD target and numerical reconstruction], 6 [Handbook of Holographic Interferometry : Optical and Digital Methods]]. It only depends on the ideal in-focus reconstruction distance, the pixel pitch and the number of pixels in the recorded hologram. When $\mathbf{U_x}$ increases (extended sensor),$|\mu|$ tends to be high for the same de state, meaning the standard deviation of noise is low. But when $\mathbf{U_x}$ decreases (narrow sensor), $|\mu|$ also decreases and the standard deviation of noise increases. That means that speckle phase decorrelation in digital Fresnel holography is closely related to the dimensions of the sensor that is used for recording holograms. The larger the sensor, the weaker the decorrelation is. Inversely, the narrower the sensor is, the higher the noise in the phase data.

2.4. Summary

In this section, we aim at summarizing the hypothesis and results of the theoretical analysis. The modeling was conducted by the evaluation of the modulus of the complex coherence factor. For that, the local surface slopes of the in-plane and out-of-plane surface deformation are the relevant parameters. These local slopes must be considered in the sense of the spatial frequencies they produce for the holographic system according to Eq. (32) :

with $\Delta\alpha_{12}$ and $\Delta\beta_{12}$ respectively the local out-of-plane and in-plane slopes due to the surface deformation between the two considered instants. The final expression of $|\mu|$, Eq.(31), depends on the simple functions `sinc and rec according to product and convolution with output variable the spatial frequencies produced by the surface slopes. The two functions respectively are related to the active surface of pixels and to the sensor dimensions. The key parameters of digital Fresnel holography are its cut-off frequencies given by the relation $(U_x, U_y) = (Np_x/\lambda d_0, Mp_y/\lambda d_0)$ in which the physical parameters are the number of pixels of the sensor (M, N) , the pixel pitch (p_x, p_y) , the distance between the object plane and the sensor (d_0), and the wavelength of light (λ) .

2.5. Case of non-extented pixels

The impact of the pixel width (represented by the sinc function in Eq.(31)) may be negligible compared to the rect function which depends on the sensor dimensions. Mathematically, that means that the sinc function of the active surface of pixels can be reduce to 1. In this case, the expression of $|\mu|$ is simply related to the two-dimensional convolution of the rectangular function, and is given by :

Here, u and v are respectively the spatial frequency in the x and y direction with $u = \frac{\Omega_z \Delta\alpha_x}{2\pi} + \frac{\Omega_x \Delta\beta_x}{2\pi}$ and $v = \frac{\Omega_z \Delta\alpha_y}{2\pi}$. Note that the curve representing Eq.(33) in the x and y directions is simply astraight line with negative slope. It follows that $|\mu|$ exhibits anisotropy according to the sensor dimensions and fringe orientation. That means $|\mu|$ depends on the inclination of the deformationsl ope with respect to the length of the sensor matrix. For the one-dimensional case, the hypothesis of the non extended pixels can be assumed by $1/\Delta_x >> N p_x/\lambda d_0$, and can also be expressed by $\sqrt{\xi} N p_x^2/\lambda d_0 << 1$. The ratio depends on experimental parameters. If d_0 increases, that is the distance between sensor and object increases, the ratio decreases and the extended surface of pixels has a reduced influence. This corresponds to the case where the spatial resolution of there constructed image is much larger than the width of the pixels. So the farther the object, the less the influence of pixel width on phase decorrelation is. This results was also pointed out in [50 [General theoretical formulation of image formation in digital Fresnel holography]]. Obviously, these rules go the other way when the object moves close to the sensor. That means that the influence of the pixel width on phase decorrelation is more significant in this case.

In order to appraise the impact of the sinc function on $|\mu|$, a simulation of the sinc and the rect functions is considered with the following parameters: $d_0 = 300\,mm$, $\lambda = 0.532\,\mu m$, $p_x = 20\,\mu m$ and $\xi = 0.58$. A comparison of the two functions with different values $\xi = 0.58$ is shown in Fig. 5(a). The width of the rectangle function compared to the sinc is relevant for $N = 512$ and $N = 1024$. That means that for these cases, the shape of the curve of $|\mu|$ is modified and is no longer a straight line with negative slope. This point is illustrated in Fig. 5(b) where $|\mu|$ is represented for the four cases $N = (128, 256, 512, 1024)$. In the last two curves for $N = 512$ and $N = 1024$, the effect of the pixel surface extension can be clearly observed since the plots become curved.

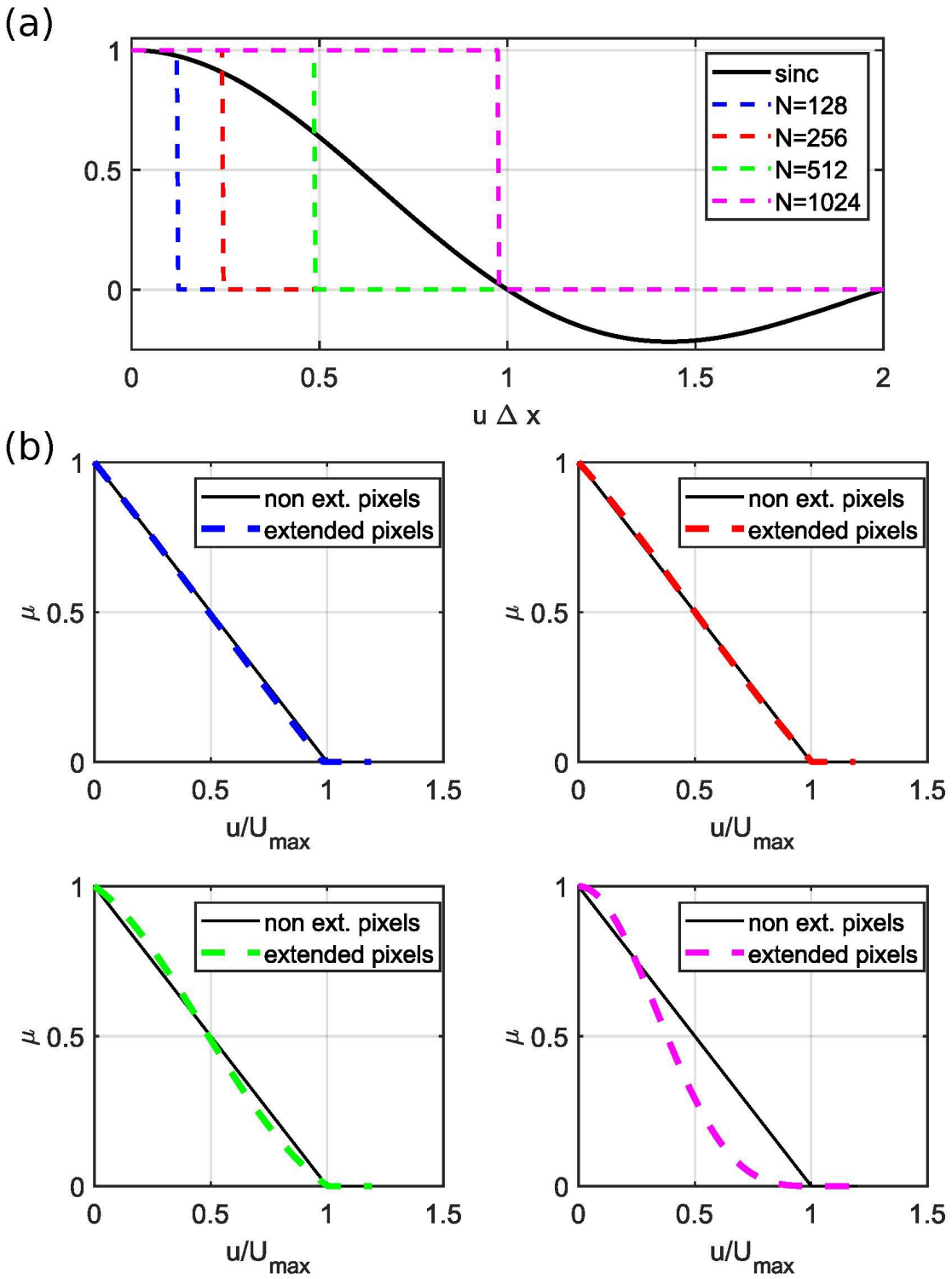

Fig. 5. (a) Comparison of the rect function from the sensor width and the sinc from the extended pixels for □=(128,256,512,1024), (b) variation of |□ | for the four cases □=(128,256,512,1024). The color code for □ in (a) is conserved in (b).

Figure 5 shows that extended pixels only modify the shape of the curve of $|\mu|$, but that they do not significantly change the sensitivity to the asymmetry of the sensor. This means that the anisotropy of noise is not modified by the extended surface of pixels. Figure 6 shows the modulus of the complex coherence factor for different cut-off frequencies of digital Fresnel holography.

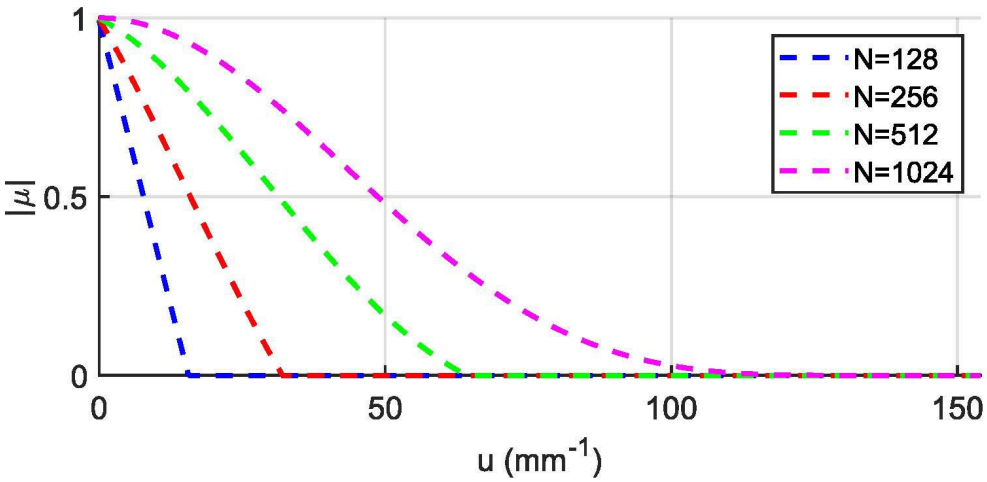

Fig. 6. Comparison of |□| for different pixels size sensor for □= (128,256,512,1024) and □0 = 300 mm, □ = 0.532 □m, □□ = 20 □m.

Next section presents a comparison between realistic numerical simulations and the theoretical expression in Eq. (31).

3. Confrontation to stimulations

3.1. Object to image simulation

Simulations of phase images are carried out in order to simulate phase maps from digital holographic Fresnel interferometry with corruption from speckle decorrelation noise. The basic scheme for the simulation is depicted in Fig. 1(c) which corresponds to the numerical implementation of the convolution equation of digital Fresnel holography (Eq.(5)). The computation is carried out using fast Fourier transforms. The initial object plane is Fourier transformed and multiplied by the Fourier transform of the PSF (Eq.(30)), and then the inverse Fourier transform yields the image plane. For the object plane, a flat surface with Gaussian roughness (standard deviation at 10λ) is numerically simulated. The object submitted to surface deformation is simulated by adding the deformation modeled as a plane with a certain slope. The slope has amplitude $\Delta\alpha$ and an orientation described by angle, ϕ so that the deformation is given by $S(x,y) = \Delta\alpha\cos(\phi)x + \Delta\alpha\sin(\phi)y$. For the sake of simplicity, only out-of-plane deformations are considered.

In order to mimic realistic practical situations, the parameters are chosen as follows : $d_0 = 2760$ mm, $\lambda = 0.532\,\mu m$, $p_x = 4.4\,\mu m$, $M = 1200$ and $N = 1600\,pixels$. The sensor is voluntary chosen having rectangular dimensions in order to highlight the anisotropy of noise, which depends on the fringe orientation. For the simulation, the pixels are considered as non-extended (fill factor close to zero). With the parameters, one has $U_{max} \simeq 4.79\,mm^{-1}$ and $V_{max} \simeq 3.59\,mm^{-1}$. By considering illumination at normal incidence ($\theta_o = \theta_e = 0$ in Fig. 4), so that $\Omega_z = 4\pi/\lambda$ and $\Omega_x = 0$, the spatial frequency of the slope has amplitude equal to $\Delta\alpha/\lambda$. The slopes are chosen so that the corresponding spatial frequencies are in the maximum range $[0, \sqrt{U_{max}^2 + V_{max}^2}]$ .This leads to $\Delta\alpha \in [0, 1.5^{-3}]$. The orientation of the fringe pattern is adjusted by varying angle ϕ from 0 to $360°$. The noisy Doppler phase is finally obtained by computing the difference between two phase maps from computation described in Fig. 1(c).

3.2. Estimation of noise

The noise maps are extracted by calculating the difference between the original noise-free and noisy phases. The standard deviation and the probability density of noise are estimated. With Eq. (9), the data are fitted to the theoretical equation in order to estimated the value of $|\mu|$.

3.3. Comparison between simulations and theory

Figure 7 presents the surface deformations as slopes in their noise-free and noisy versions for 5 inclination angles $\phi = (0, 30, 45, 60, 90)°$.

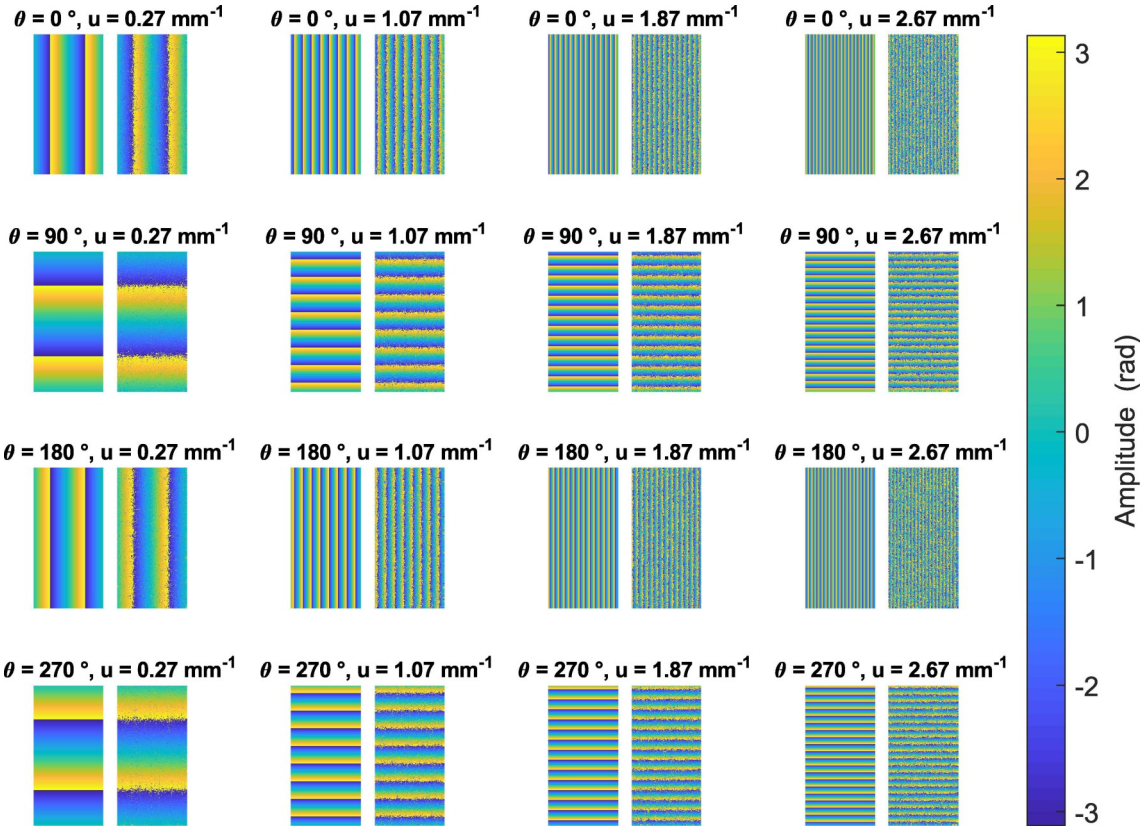

Fig. 7. Extractions from the simulator for surface deformations as slopes. The modulo 2□ phase maps are given for 5 inclination angles (0, 30, 45, 60, 90) and progressive spatial frequencies from 0.01 □□−1 to 0.08 □□−1. Noise-free and noisy surface deformations are displayed for each case.

Figure 8 shows the comparisons between the values of $|\mu|$ estimated from the simulated noisy phase maps and that obtained with theory from Eq.(33). As can be observed, the simulation is in very good agreement with the theoretical expression. This confirms that the decorrelation noise is sensitive to the orientation of the fringes when the sensor exhibits asymmetry such as rectangular formats.

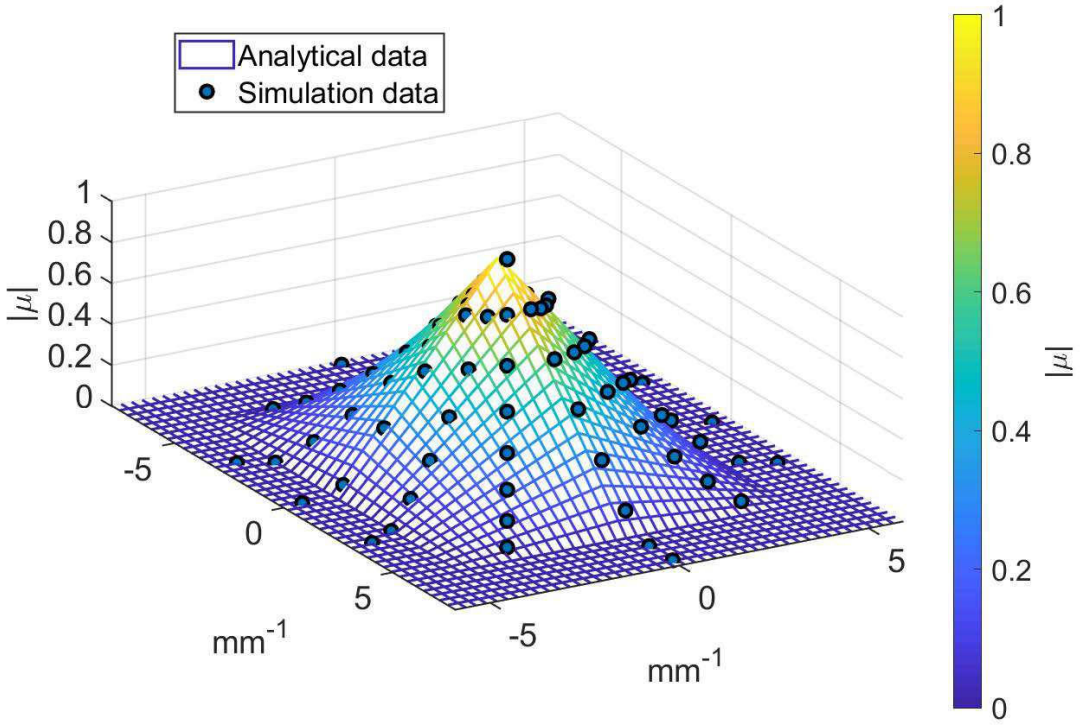

Fig. 8. Comparison between the analytical expression from Eq.(33) and the simulation results for different values of the slope amplitude and orientation.

4. Experiments

4.1. Experimental set-up

In this section, comparison between analytical and experimental results is provided. The experimental set-up is presented in Fig. 9 (a). The object surface and the camera sensor are illuminated by a continuous green laser (wavelength $\lambda = 532\ nm, 6\ W$ maximum power). The light emitted by the laser is split by a polarizing beam splitter (PBS) to produce the reference and illumination beams. The object wave is spatially expanded to illuminate the structure by using a dedicated DOE (Diffractive Optical Element) [57 [Applied digital optics: from micro-optics to nanophotonics]]. The DOE was designed with 8 subareas, each of them producing a particular laser beam shape [58 [Versatile stepper based maskless microlithography using a liquid crystal display for direct write of binary and multilevel microstructures]]. Figure 9 (b) illustrates the diversity of shapes that can be produced with the DOE : square area, elliptical areas, narrow and large rectangular beams (vertical and horizontal). Such beam shaping increases the photometry efficiency of the set-up by avoiding wasting light with classical lenses and mirror assembly. For further details on the realization of the DOE, the reader is invited to consider [59 [Combined digital-DOE holographic interferometer for force identifcation in vibroacoustics]]. The sensor is from SONY ICX274AL and is inserted in a Imaging Source DMK 51buc02 camera. The pixel size is at $p_x = p_y = 4.4\ \mu m$ and maximum resolution is at 1200×1600 pixels. The exposure time is set at $100\ \mu s$ and the configuration is off-axis digital Fresnel holography. The illumination beam impacts the object surface with angle $\theta_e = 15$ degrees and observation is at normal incidence $(\theta_o = 0)$, so that $\Omega_z \simeq 1.96\pi/\lambda$.

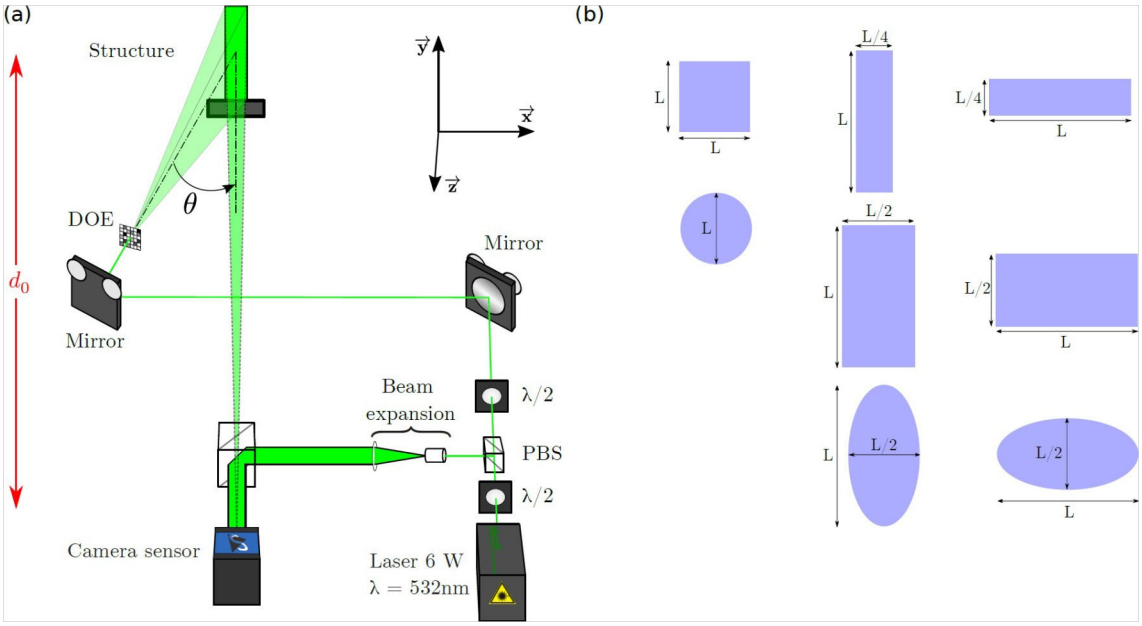

Fig. 9. (a) Experimental set-up for full-field holographic vibrometry (PBS : polarizing beam splitter, DOE : Diffractive Optical Element, □/2 half-wave plate), (b) set of beam shape structures that can be produced by the DOE to illuminate the object surface. The z axis is oriented along the propagation of the light beam from the structure plane and the x-y axes are parallel to the structure plane.

For the comparison with theory, the tested object is a rectangular aluminum beam sized $26,4$ cm high, $2,03$ cm wide and $0,49$ cm thick. The distance between sensor and object is set at $d_0 \simeq 2760\ mm$. This yields $U_{max} = 4.79\ mm^{-1}$ and $V_{max} = 5.59\ mm^{-1}$. The mechanical beamis submitted to a load force that produces bending and then a displacement. This is done using ascrew with micrometric accuracy at one of its extremity, whereas the other one is clamped to

the optical table. The precision screw is embedded in a non-deformable heavy beam, so that the screw will push the structure and apply a controlled static force to the top of the beam.

Note that submitting the beam to load force at its extremity induces out-of-plane deformations. The advantage of such mechanical configuration is that the bending of the beam produces straightand parallel fringes. It follows that, in this set-up, the comparison is carried out by consideringout-of-plane experimental deformations, such that there is no contribution from any in-plane movement. The mechanical beam is oriented in three positions, at 0 degree (horizontal beam), at 45 degrees and finally at 90 degrees (vertical beam). These three configurations are well suitedfor exhibiting the noise anisotropy of the holographic arrangement. Figures 10(a)-10(c) show schemes of the aluminum beam for the three orientations.

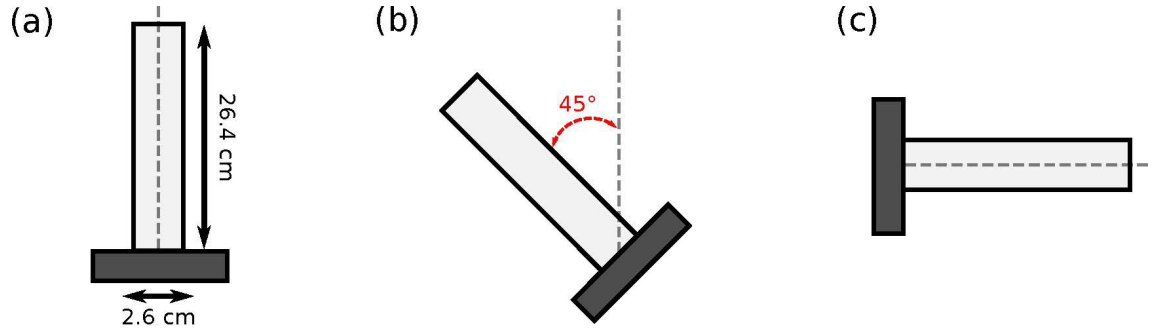

Fig. 10. Schemes for the three positions of the aluminum beam oriented at, (a) 90 degree for the vertical beam, (b) 45 degrees, (c) 0 degrees for the horizontal beam.

4.2. Data processing

Sets of digital holograms are recorded for the three beam inclinations when progressively applying the load force to the beam, starting from no load to a maximum load enabling fringe patterns to be processed. Then, the digital holograms are numerically reconstructed and the phase are extracted to compute the Doppler phases between the current load state and the initial static state . From that, a set of noisy phase fringe patterns is obtained. In order to estimate the experimental slope due to deformation, and thus the corresponding spatial frequency, robust and error-reducedde-noising using the 2-D windowed Fourier transform is performed [31 [Quantitative appraisal for noise reduction in digital holographic phase imaging],52 [Two-dimensional windowed Fourier transform for fringe pattern analysis: Principles, applications and implementations],60 [Error analysis for noise reduction in 3D deformation measurement with digital color holography]]. The de-noised phase maps are then unwrapped and converted into physical data (multiplication by $\lambda/3.92\pi$) in order to estimate the slope of the surface deformation. The surface slope is estimated using least square minimization when fitting data with $\Delta\alpha_x x + \Delta\alpha_y y$. From $(\Delta\alpha_x, \Delta\alpha_y)$ the spatial frequencies of the slope are estimated. With the de-noised phase data, the decorrelation noise can be estimated by subtraction of the raw phase. Then, the probability density function and the modulus of the complex coherence factor are estimated. Note that the slope estimation is performed on local patches mapping the beam in order to get local slope estimations and local estimates of $|\mu|$. Similarly, for each patch over which the slope deformation is measured, the value of $|\mu|$ is obtained.

4.3. Experimental results

The recording of the holograms is carried out with the native resolution of 1200×1600 pixels. Figure 11 shows the image amplitudes of the reconstructed holograms in the three different inclinations. The off-axis images can be appreciated. For each beam inclination, Fig. 11 provides raw phase maps in which the progressive fringe density increases from the foot (clamped beam) to the top of the beam (load force).

These raw data are then processed to get estimations of the noise, the slope and finally of $|\mu|$.

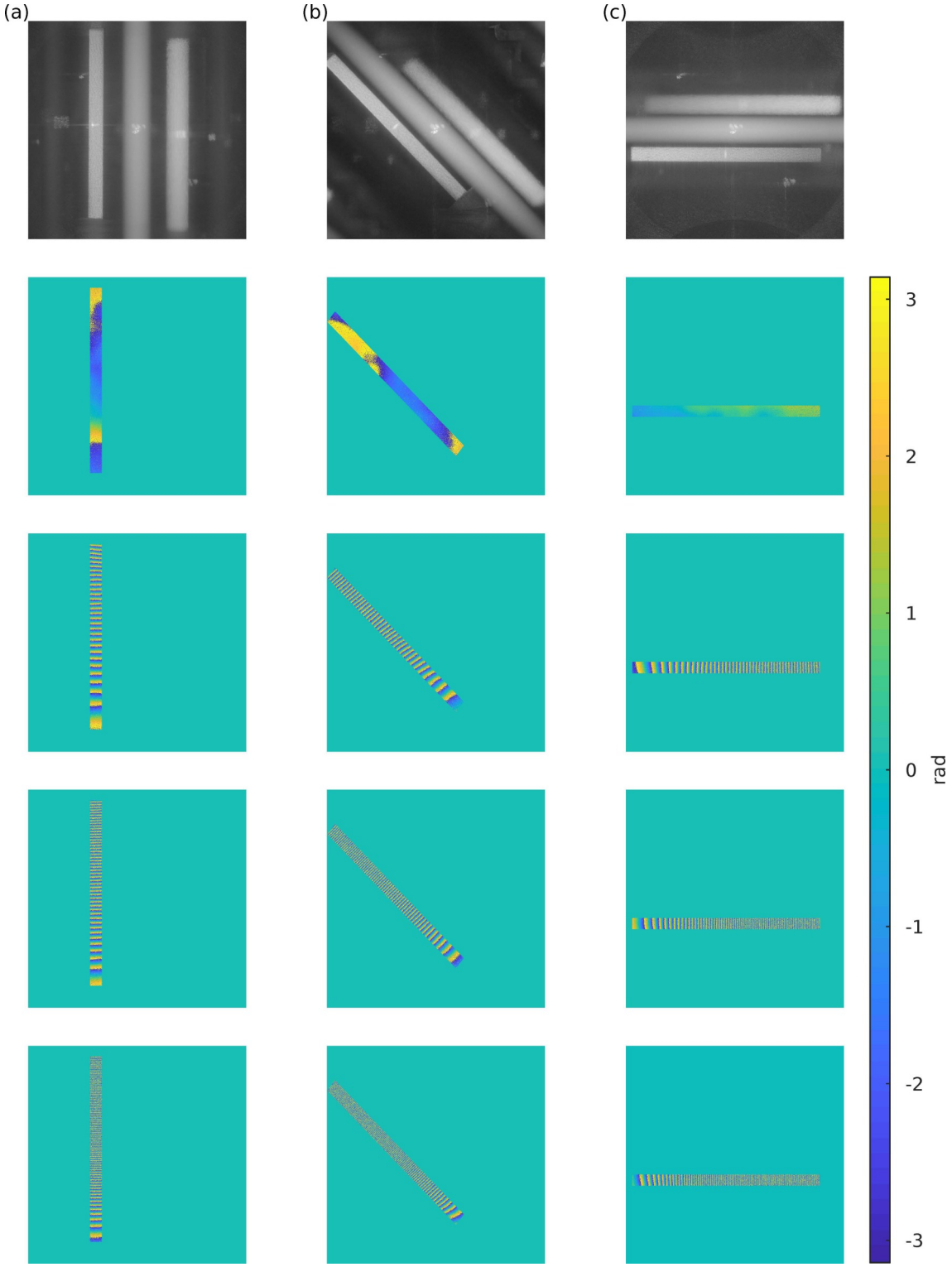

Fig. 11. Examples of reconstructed amplitudes and phase maps for the three beam inclinations, (a) vertical beam, (b) beam oriented at 45 degrees, (c) horizontal beam . Four phase images for four different bending are provided.

The theoretical profile of $|\mu|$ is recalled in Fig. 12(a) and the three orientations of the beam are highlighted, respectively with the dashed blue line for the horizontal beam, the dashed red line for the vertical orientation and the dashed green line for the inclined one. Figures 12(b)-12(d)

show the comparison between the theoretical $|\mu|$ and the experimental results respectively for the vertical beam, the horizontal beam and the inclined beam.

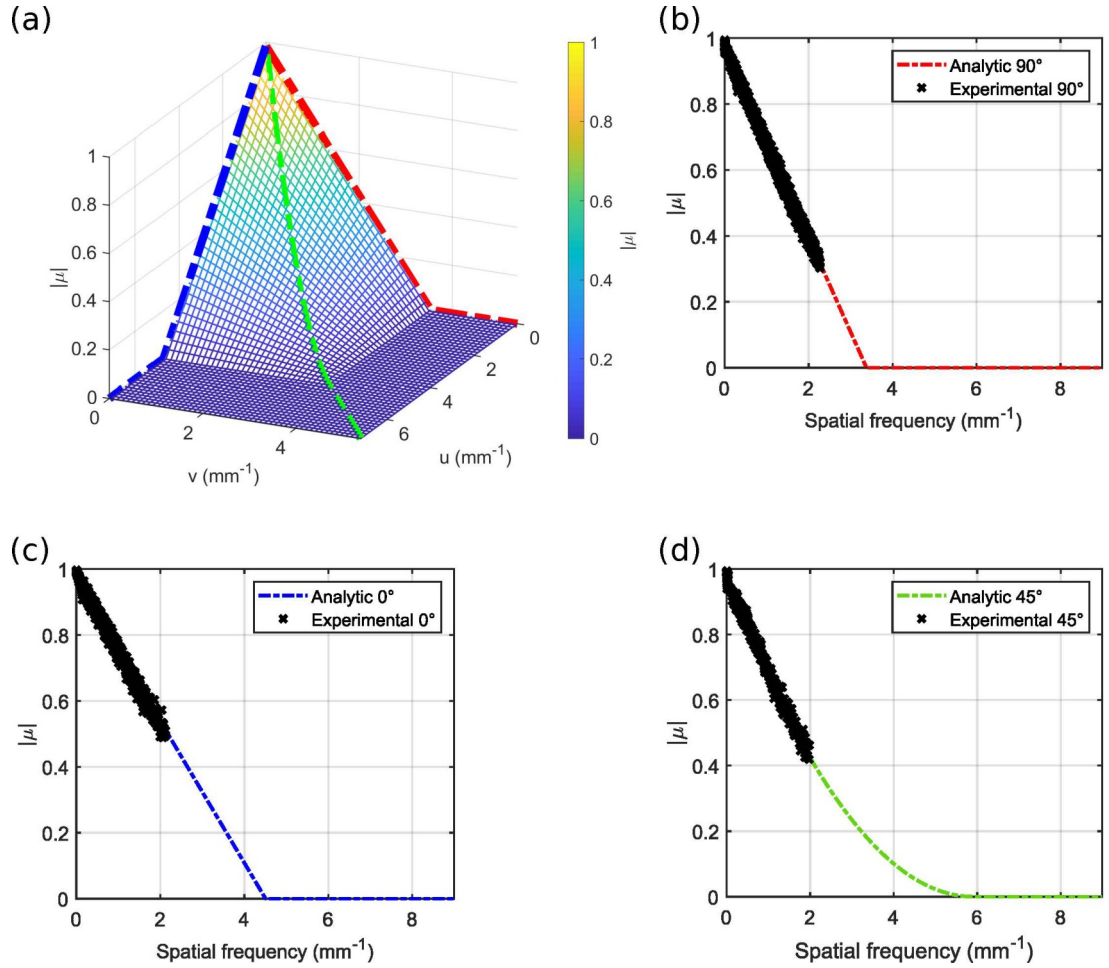

Fig. 12. Comparison between theory and experiments, (a) theoretical values of |□|, with the dashed blue line for the horizontal beam, the dashed red line for the vertical orientation and the dashed green line for the inclined one, (b) comparison between experimental estimations of |□| and theoretical values for the case of the vertical beam, (c) comparison between experimental estimations of |□| and theoretical values for the case of the horizontal beam, (d) comparison between experimental estimations of |□| and theoretical values for the case of the inclined beam.

Figure 12 shows the very good agreement between the theoretical expression in Eq. (31) and the experimental results. Note that from the experimental point of view, values of $|\mu|$ lower than 0.3 are difficult to reach. This is why plots in Fig. 12(b)-(c) do not exhibit values of $|\mu|$ down to 0. When $|\mu|$ decreases, the fringe density increases and requires that phase jumps are sampled withat least 4 pixels per phase jump. In addition, the de-noising algorithm also requires a minimum of sampling data points to operate or this is not possible to process data further. Note that, in an near future, more powerful de-noising algorithms could eventually be considered for very low values of μ, such as new approaches provided by deep learning [61 [Towards reduced cnns for de-noising phase images corrupted with speckle noise]]. The results in Fig. 12 confirm that the modulus of the complex correlation factor is closely related to the slope of the surface deformation.

The theoretical value of $|\mu|$ depends on the parameters of the experimental set-up and especially of the width of the sensor in the Fresnel configuration. These results also demonstrate the importance of carrying out holographic measurements at high spatial sensor resolution because the decorrelation noise will be lower compared to reduced sensor spatial extension.

La valeur théorique de $|\mu|$dépend des paramètres du dispositif expérimental et notamment de la largeur du capteur dans la configuration de Fresnel. Ces résultats démontrent également l'importance d'effectuer des mesures holographiques à haute résolution spatiale du capteur, car le bruit de décorrélation sera inférieur à celui d'une extension spatiale réduite du capteur.

* *

*

This course provides the theoretical expression of the modulus of the coherence factor controlling the speckle noise decorrelation in measurements from digital holographic interferometry. As main result, the correlation coefficient depends on the geometrical characteristics of the set-up such as the number of pixels of the recording matrix, the size and pitch of the pixels, the illumination wavelength, the distance between object and sensor, and the local slope of thes urface deformation between the two considered instants. The theoretical analysis shows that the decorrelation is anisotropic and depends on both the local phase fringe pattern orientation and the widths of the sensor. The theory is confronted to realistic simulations confirming the relevance of the proposed analysis. Experiments are carried out for the case of a mechanical beam submitted to bending with a load force. From the digitally reconstructed holograms, the phase fringe patterns for three different orientations of the mechanical beam are processed and the local slopes of the induced surface deformations are evaluated. From those data, the modulus of the complex coherence factor is estimated. Experimental results confirm the very good agreement with the theoretical modeling and demonstrate the anisotropic characteristic of the decorrelation phase noise in digital Fresnel holography.

The interpretation of the theory can be approached from the point of view of spatial frequencies. In the Fresnel configuration, it can be considered that the sensor, due to its limited spatial extension, behaves as a low-pass filter and attenuates the high spatial frequencies corresponding to the strong slopes of the surface deformation. It follows that the speckle decorrelation noise is related to the modulation transfer function of digital Fresnel holography and that noise increases if the local slope of surface deformation increases. Holographic imaging, as a linear filtering between the physical object and the digitally reconstructed image, disturbs the propagation of the spatial frequencies related to the deformation slope and this has for consequence the increase of the speckle decorrelation in the Doppler phase. Consequently, the attenuation results in phase noise in the measured phase fringe pattern between the two considered instants. The results presented in this course open the way to new advanced approaches of de-noising indigital holographic metrology by considering prior knowledge on the surface deformation in order to predict the local noise and to adapt the noise processing. This would be very useful forhigh-speed holographic imaging in which the number of pixels of the sensor is reduced and the decorrelation noise higher than in conventional experiments.

Bibliographie

[A new Microscopic Principle] D. Gabor,*"A New Microscopic Principle,"* Nature. 161, 777-778 (1948).

[Application of speckle-correlation methods to surface-roughness measurement: a theoretical study] B. Rufng, "*Application of speckle-correlation methods to surface-roughness measurement: a theoretical study,"* J. Opt. Soc. Am. A 3, 1297–1304 (1986).

[Applied digital optics: from micro-optics to nanophotonics] B. C. Kress and P. Meyrueis, *Applied digital optics: from micro-optics to nanophotonics* (Wiley, Chichester, U.K, 2009).

[Calculation of complex correlation coefficents of two speckle fields of different wavelengths, and their application to two-wavelength-measurement techniques] U. Vry, "Calculation of complex correlation coefficents of two speckle fields of different wavelengths, and their application to two-wavelength-measurement techniques," J. Opt. Soc. Am. A 5, 114-125 (1988).

[Combined digital-DOE holographic interferometer for force identifcation in vibroacoustics] J. Poittevin, C. Faure, J. Le Meur, P. Picart, C. Pezerat, and K. Heggarty, "Combined digital-DOE holographic interferometer for force identifcation in vibroacoustics," Procedings SPIE 10677, 106773A (2018).

[Comparative analysis of autofocus functions in digital in-line phase-shifting holography] E. S. Fonseca, P. T. Fiadeiro, M. Pereira, and A. Pinheiro, "*Comparative analysis of autofocus functions in digital in-line phase-shifting holography,*" Appl. Opt. 55. 7663-7674 (2016).

[Comparative study of multi-look processing for phase map de-noising in digital Fresnel holographic interferometry] S. Montrésor, P. Memmolo, V. Bianco, P. Ferraro, and, P. Picart,*"Comparative study of multi-look processing for phase map de-noising in digital Fresnel holographic interferometry,"* J. Opt. Am. A 36, A59-A66 (2019).

[Decorrelation and fringe visibility : on the limiting behavior of various electronic speckle-pattern correlation interferometers] M. Owner-Petersen, *"Decorrelation and fringe visibility: on the limiting behavior of various electronic speckle-pattern correlation interferometers,"* J. Opt. Soc. Am. A 8, 1082–1089 (1991).

[Deformation measurement by phase-shifting digital holography] Y. Morimoto, T. Nomura, M. Fujigaki, S. Yoneyama, and I. Takahashi, *"Deformation measurement by phase-shifting digital holography,"* Exp. Mech. 45, 65-70 (2005).

[Digital double pulse-TV holography] G. Pedrini, H. J. Tiziani, and Y. Zou, *"Digital double pulse-TV holography,"* Opt. Lasers Eng. 26, 199-219 (1997).

[Digital holography and three-dimensional display : Principles and Applictions] T.-C. Poon,*Digital holography and three-dimensional display : Principles and Applictions* (Springer Science & Business Media, 2006).

[Digital stroboscopic holography setup for deformation measurement at both quasi-static and acoustic frequencies] D. De Greef, J. Soons, and J. J. Dirckx,*"Digital stroboscopic holography setup for deformation measurement at both quasi-static and acoustic frequencies,"* Int. J. Optomechatronics, 8, 275-291 (2014).

[Direct recording of hologram by a a CDD target and numerical reconstruction] U. Schnars and W. Jüptner, *"Direct recording of hologram by a a CDD target and numerical reconstruction,"* Appl. Opt. 33., 179-181 (1994).

[Error analysis for noise reduction in 3D deformation measurement with digital color holography] S. Montrésor, P. Picart, O. Sakharuk, and L. Muravsky, *"Error analysis for noise reduction in 3D deformation measurement with digital color holography,"* J. Opt. Soc. Am. B 34, B9–B15 (2017).

[Experimental and theroretical of the pixel saturation effect in digital holography] P. Picart, P. Tankam, and Q. Song, *"Experimental and theroretical of the pixel saturation effect in digital holography,"* J. Opt. Soc. Am. A 28, 1262-1275 (2011).

[First-order probability density function of the laser speckle phase] J. Uozumi and T. Asakura, *"First-order probability density function of the laser speckle phase,"* Opt. Quantum Electron. 12, 477–494 (1980).

[General analysis of fringe contrast in electonic speckle pattern interferometry] G. A. Slettemoen, *"General analysis of fringe contrast in electonic speckle pattern interferometry,"* Opt. Acta : Int. J. Opt. 26, 313-327 (1979).

[General theoretical formulation of image formation in digital Fresnel holography] P. Picart and J. Leval, *"General theoretical formulation of image formation in digital Fresnel holography,"* J. Opt. Soc. Am. A, JOSAA 25, 1744–1761 (2008).

[Handbook of Holographic Interferometry : Optical and Digital Methods] T. Kreis, *Handbook of Holographic Interferometry : Optical and Digital Methods* (Wiley, 2004), 1st ed.

[High-resolution quantitative phase-contrast microscopy by digital holography] C. J. Mann, L. Yu, C. M. Lo, and M.K. Kim, *"High-resolution quantitative phase-contrast microscopy by digital holography,"* Opt. Express 13, 8693-8698 (2005).

[Holographic tomography : techniques and biomedical applications] V. Balasubramani, A. Kuś , H.-Y. Tu, C.-J. Cheng, M. Baczewska, W. Krauze, and M. Kujawińska, *"Holographic tomography : techniques and biomedical applications,"* Appl. Opt. 60, B65-B80 (2021).

[Inline application of digital holography] M. Fratz, T. Beckmann, J. Anders, A. Bertz, M. Bayer, T. Giessler, C. Nemeth, and D. Carl, *"Inline application of digital holography,"* Appl. Opt., 58, G120-G126 (2019).

[Introduction To Fourier Optics] J. W. Goodman, *Introduction To Fourier Optics* (W.H.Freeman & Co Ltd, Englewood, Colo, 2005).

[Laser speckle and related phenomena] J. C. Dainty, ed., *Laser speckle and related phenomena*, no. 9, in Topics in applied physics (Springer, Berlin, 1984), 2nd ed.

[Lock-in vibration retrieval based on high-speed full-field coherent imaging] E. Meteyer, S. Montresor, F. Foucart, J. Le Meur, K. Heggarty, C. Pezerat, and P. Picart,*"Lock-in vibration retrieval based on high-speed full-field coherent imaging,"* Sci. Reports 11, 7026-7040 (2021).

[Maximal fraction of acceptable measurements in phase-shifting speckle interferometry: a theoretical study] G. A. Slettemoen and J. C. Wyant, *"Maximal fraction of acceptable measurements in phase-shifting speckle interferometry: a theoretical study,"* J. Opt. Soc. Am. A 3, 210–214 (1986).

[Measurement of the integral refractive index and dynamic cell morphometry of living cells with digitalholographic microscopy] B. Rappaz, P. Marquet, E. Cuche, Y. Emery, C. Depeursinge, and P. J. Magistretti,*"Measurement of the integral refractive index and dynamic cell morphometry of living cells with digital holographic microscopy,"* Opt. Express 13, 9361-9373 (2005). Publisher : OSA.

[Measuring shape and deformation of small objects using digital holography] S. Seebacher, W. Osten, and W. P. Jueptner, "Measuring shape and deformation of small objects using digital holography," in *Laser Interferometry IX : Applications,* vol. 3479 (International Society for Optics and Photonics, 1998), pp. 104-115.

[Mechanical behavior of CAD/CAM occlusal ceramic reconstruction assessed by digital color holography] H. Xia, M. Secail-Geraud, J. Le Meur, S. Montresor, K. Heggarty, C. Pezerat, and P. Picart,*"Mechanical behavior of CAD/CAM occlusal ceramic reconstruction assessed by digital color holography,"* Dental Mater. 34, 1222-1234 (2018).

[Miniaturized digital holography sensor for distal three-dimensional endoscopy] E. Kolenovic, W. Osten, R. Klattenhoff, S. Lai, C. v. Kopylow, and W. Jüptner,*"Miniaturized digital holography sensor for distal three-dimensional endoscopy,"* Appl. Opt. 42, 5167-5172 (2003).

[Multi-point vibrometer based on high-speed digital in-line holography] J. Poittevin, P. Picart, C. Faure, F. Gautier, and C. Pézerat,*"Multi-point vibrometer based on high-speed digital in-line holography,"* Appl. Opt. 54, 3185-3196 (2015).

[New techniques in digital holography] P. Picard, ed., *New techniques in digital holography, Instrumentation and measurement series* (ISTE Ltd ; John Wiley & Sons., Inc, London, 2015).

[New techniques in wavefront reconstruction] E. N. Leith and J. Upatnieks, *"New techniques in wavefront reconstruction, "* J. Opt. Soc. Am 51, 1469-1473 (1961).

[Quality assement of refocus criteria for particle imaging in digital off-axis holography] S. K. Mohammed, L. Bouamama, D. Bahloul, and P. Picart,*"Quality assement of refocus criteria for particle imaging in digital off-axis holography,"* Appl. Opt. 56, F158-F166 (2017).

[Quality assessment of combined quantiziation-shot-noise induced decorrelation noise in high-speed digital holographic metrology] J. Poittevin, P. Picart, F. Gautier, and C. Pezerat, *"Quality assessment of combined quantiziation-shot-noise induced decorrelation noise in high-speed digital holographic metrology,"* Opt. Express. 23, 30917-30932 (2015).

[Quantitative appraisal for noise reduction in digital holographic phase imaging] S. Montresor and P. Picart, *"Quantitative appraisal for noise reduction in digital holographic phase imaging,"* Opt. Express 24, 14322-1434 (2016).

[Quasi noise-free digital holography] V. Bianco, P. Memmolo, M. Paturzo, A. Finizio, B, Javidi, and P. Ferraro,*"Quasi noise-free digital holography",* Light. Sci Appl 5, e16142-e1642 (2016).

[Reduction of speckle in digital holography by discrete Fourier filtering] J. Maycock, B. M. Hennelly, J. B. McDonald, Y. Frauel, A. Castro, B. Javidi, and T. J. Naughton, *"Reduction of speckle in digital holography by discrete Fourier filtering,"* J. Opt. Soc. Am. A 24, 1617-1622 (2007).

[Reduction of speckle noise in multiwavelength contouring] C. Falldorf, S. Huferath-von Luepke, C. Von Kopylow, and R. B. Bergmann,*"Reduction of speckle noise in multiwavelength contouring,"* Appl. Opt, 51, 8211-8215 (2012).

[Refocus criterion based on maximization of the coherence factor in digital three-wavelenght holographic interferometry] P. Picart, S. Montresor, O. Sakharuk, and L. Muravsky, *"Refocus criterion based on maximization of the coherence factor in digital three-wavelenght holographic interferometry, "* Opt. Lett. 42 275-278 (2017).

[Refocusing criterion via sparisty measurements in digital holography] P. Memmolo, M. Paturzo, B. Javidi, P. A. Netti and P. Ferraro, *"Refocusing criterion via sparisty measurements in digital holography,"* Appl. Opt. 39, 4719-4722 (2014).

[Remote metrology by comparative digital holography] T. Baumbach, W. Osten, C von Kopylow, and W. Jüptner, *"Remote metrology by comparative digital holography,"* Appl. Opt. 45, 925-934 (2006).

[Roughness determination by speckle-wavelength decorrelation] D. J. Schertler and N. George, *"Roughness determination by speckle-wavelength decorrelation,"* Opt. Lett. 18, 391-393 (1993).

[Separate recording of rationally related vibration frequencies using digital stroboscopic holographic interferometry] I. Alexeenko, M. Gusev, and V. Gurevich, *"Separate recording of rationally related vibration frequencies using digital stroboscopic holographic interferometry,"* Appl. Opt. 48, 3475-3480 (2009).

[Some opportunities for vibration analysis with time averaging in digital Fresnel holography] P. Picart, J. Leval, D. Mounier, and S. Gougeon, *"Some opportunities for vibration analysis with time averaging in digital Fresnel holography,"* Appl. Opt. 44, 337–343 (2005).

[Space and wavelength dependence of speckle intensity] N. George and A. Jain, *"Space and wavelength dependence of speckle intensity,"* Appl. Phys. 4, 201–212 (1974).

[Speckle at various plane in an optical system] N. George, *"Speckle at various plane in an optical system,"* Opt. Eng. 25, 256754 (1986).

[Speckle decorrelation in surface profilometry by wavelength scanning interferometry] I. Yamaguchi, A. Yamamoto, and S. Kuwamura, *"Speckle decorrelation in surface profilometry by wavelength scanning interferometry,"* Appl. Opt. 37, 6721-6728 (1998).

[Speckle Phenomena in Optics : Theory and Applications] J. W. Goodman, *Speckle Phenomena in Optics : Theory and Applications,* Second Edition (SPIE, 2007).

[Spectral correlation of partially or fully developped patterns generated by rough surfaces] B. Ruffing and J. Fleisher, "*Spectral correlation of partially or fully developped patterns generated by rough surfaces,"* J. Opt. Soc. Am. A 2, 1637-1643 (1985).

[Statistical optics] J. W. Goodman,*Statistical optics* (Wiley, New York, 2000).

[Surface-roughness neasurement based on the intensity correlation function of scattered light under speckle-pattern illumination] P. Lehmann, *"Surface-roughness neasurement based on the intensity correlation function of scattered light under speckle-pattern illumination,"* Appl. Opt. 38, 1144-1152 (1999).

[Surface topography measuremnt by frequency sweeping digital holography] V. Lédl, P. Psota, F. Kaván, O. Matoušek, and P. Mokrý, *"Surface topography measuremnt by frequency sweeping digital holography,"* Appl. Opt. 56, 7808-7814 (2017).

[Theoretical analysis of surface-shape-induced decorrelation noise in multi-wavelength digital holography] M. Piniard, B Sorrente, G. Hug, and P. Picart, *"Theoretical analysis of surface-shape-induce decorrelation noise in multi-wavelength digital holography,"* Opt. Express 29, 14720-14735 (2021).

[Three-dimensional micrscopy with phase-shifting digital holography] T. Zhang and I. Yamaguchi, *"Three-dimensional micrscopy with phase-shifting digital holography,"* Opt. Lett. 23, 1221-1223 (1998).

[Towards reduced cnns for de-noising phase images corrupted with speckle noise] M. Tahon, S. Montresor, and P. Picart, *"Towards reduced cnns for de-noising phase images corrupted with speckle noise,"* Photonics 8, 255 (2021).

[Transient vibration measurements using multi-pulse digital holography] G. Pedrini, P. H. Fröning, H. Fessler, and H. Tiziani, *"Transient vibration measurements using multi-pulse digital holography,"* Opt. & Laser Technol. 29, 505-511 (1998).

[Twin-sensitivity measurement by spatial multiplexing of digitally recorded holograms] P. Picart, E. Moisson, and D. Mounier,*"Twin-sensitivity measurement by spatial multiplexing of digitally recorded holograms,"* Appl. Opt. 42, 1947-1957 (2003).

[Two-dimensional windowed Fourier transform for fringe pattern analysis: Principles, applications and implementations] Q. Kemao, *"Two-dimensional windowed Fourier transform for fringe pattern analysis: Principles, applications and implementations,"* Opt. Lasers Eng. 45, 304–317 (2007).

[Versatile stepper based maskless microlithography using a liquid crystal display for direct write of binary and multilevel microstructures] M. V. Kessels, M. El Bouz, R. Pagan, and K. Heggarty,*"Versatile stepper based maskless microlithography using a liquid crystal display for direct write of binary and multilevel microstructures,"* J. Micro/Nanolith. MEMS MOEMS 6, 033002 (2007).

[Visualization of travelling waves propagating in a plate equipped with 2D ABH using wide-field holographic vibrometry] L. Lagny, M. Secail-Geraud, J. Le Meur, S. Montresor, K. Heggarty, C. Pezerat, and P. Picart,*"Visualization of travelling waves propagating in a plate equipped with 2D ABH using wide-field holographic vibrometry,"* J. Sound Vib. 461, 114925 (2019).